SUPPLEMENTARY DATA

Materials and Methods

Reverse phase protein array (RPPA)

Cell pellets contaning 5 x 10^6 cells were used for RPPAs of ibrutinib-sensitive/ibrutinib-resistant (IR) pairs through the MD Anderson RPPA core facility. In brief, cells were washed twice with ice-cold phosphate-buffered saline supplemented with a phosphatase-inhibitor cocktail (PhosStop, Roche Applied Science) and 1 mmol/L sodium orthovanadate. Samples were serially diluted 2-fold for 5 dilutions and arrayed on nitrocellulose-coated slides in an 11x11 format containing 303 unique antibodies. Relative protein levels for each sample in the RPPA analysis were determined by interpolation of each dilution curve from the "standard curve" using R package SuperCurve. All data points were normalized for protein loading and transformed to linear values. Normalized linear values were transformed to log2 values, and then median-centered for hierarchical cluster analysis and heat map generation (in Cluster 3.0 [http://cluster2.software.informer.com/3.0/] as a hierarchical cluster using Pearson correlation and a center metric). The resulting heat map was visualized in Treeview http://rana.lbl.gov/EisenSoftware.htm) and presented in a high-resolution bmp format. All data points were normalized for protein loading and transformed to a linear value.

FRET Activity

AKT activity was measured using genetically coded AKT activity biosensor as reported previously. [1] Briefly, AKT-activity reporter is a Förster Resonance Energy Transfer (FRET) based biosensor containing donor Cerulean3 fluorescence protein and acceptor cpVenus E172 separated by a FHA1 domain, flexible linker and a FOXO1 phosphorylation site (FOXO1 is a natural AKT target): the Lyn-Akt-AR2-EV biosensor. Upon phosphorylation of the FOXO1 site by AKT, the biosensor changes its conformation resulting in FRET efficiency increase. Therefore, the FRET changes correspond to the changes in AKT activity. FRET changes were measured using flow cytometry and data was processed using an in-house R script as previously reported.[1] HBL1 cell line was transduced to stably express the AKT biosensor using the Sleeping beauty transposon system. [2] For knock-out, the CRISPR/Cas9 system was used. [3,4]

Research Resource Identifiers for cell lines

1. HBL1: RRID:CVCL_4213
2. OCI-LY-10 : RRID:CVCL_8795
3. TMD8: RRID:CVCL_A442

4. OCI-LY3: DSMZ Cat# ACC-761, RRID:CVCL_8800
5. U2932: DSMZ Cat# ACC-633, RRID:CVCL_1896
6. SU-DHL-8: DSMZ Cat# ACC-573, RRID:CVCL_2207
7. OCI-LY-7: DSMZ Cat# ACC-688, RRID:CVCL_1881
8. OCI-LY-1 DSMZ Cat# ACC-722, RRID:CVCL_1879
9. OCI-LY-8 RRID:CVCL_8803
10. SU-DHL-6 ATCC Cat# CRL-2959, RRID:CVCL_2206

Chemical Abstracts Service chemical structures

1. Alpelisib 1217486-61-7
2. AZD 6482 1173900-33-8
3. Ibrutinib (PCI-32765) 936563-96-1
4. Idelalisib 870281-82-6
5. Pictilisib 957054-30-7
6. KA2237 CUI CL504848
   (https://ncim.nci.nih.gov/ncimbrowser/ConceptReport.jsp?dictionary=NCI%20Metathesaurus&code=CL504848)

Supplementary Figures

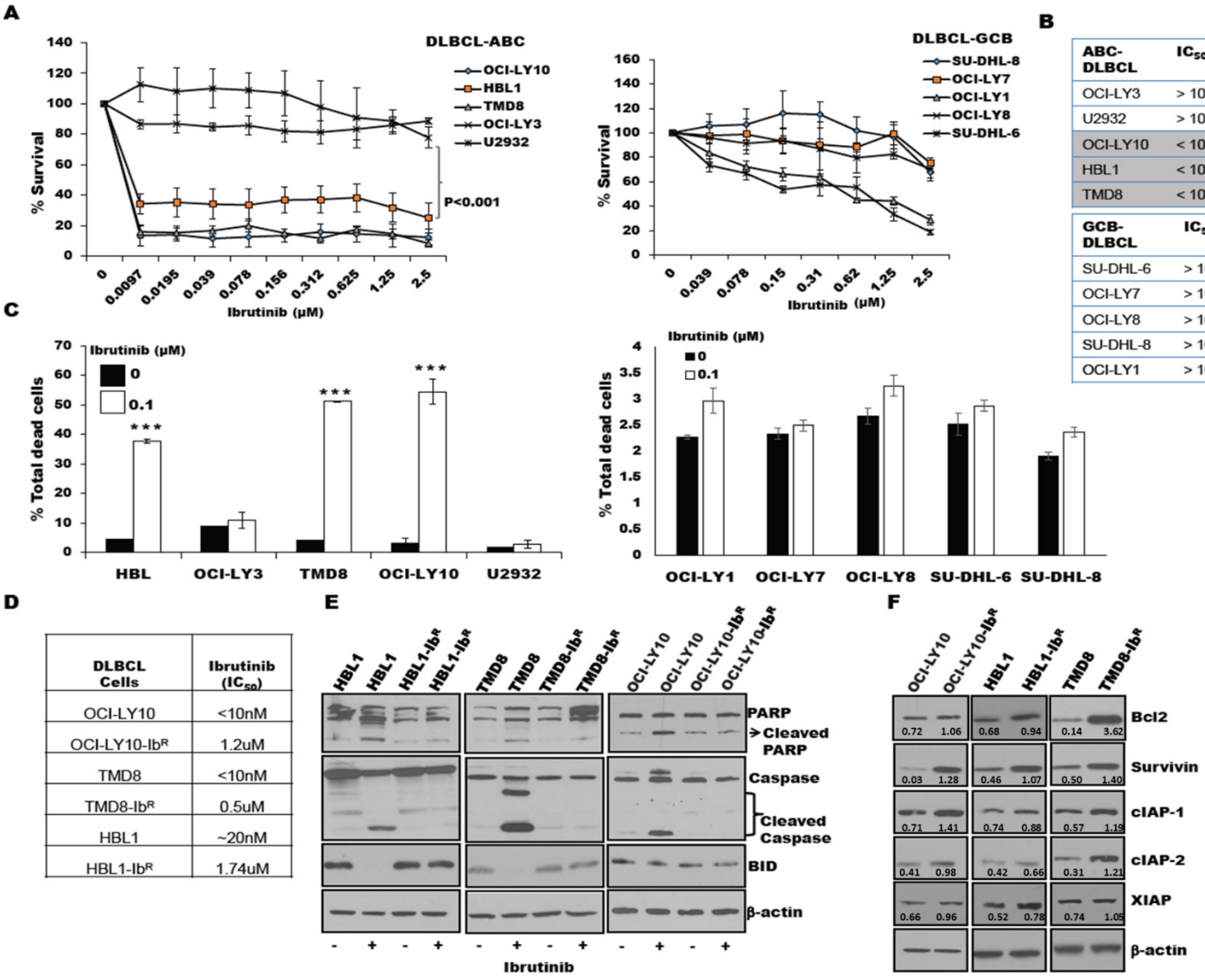

Figure S1.

IR-DLBCL cells and cell proliferation. **A,** Five ABC- and five GCB subtypes of DLBCL cell lines were treated with increasing concentrations of ibrutinib; cell growth was analyzed using an MTT cell proliferation assay. **B,** This table lists IC_{50} values of DLBCL cell lines exposed to ibrutinib. **C,** Total percentage of dead cells in DLBCL cell lines after treatment with ibrutinib (*** $p<0.001$). **D,** IC_{50} values of IR-DLBCL cells after generation of resistance. **E,** Western blots for PARP and caspase cleavage after ibrutinib treatment of parental/IR-DLBCL pairs. **F,** Western blots analysis for the IAP family members in parental/IR pairs along with the densitometry values normalized to actin.

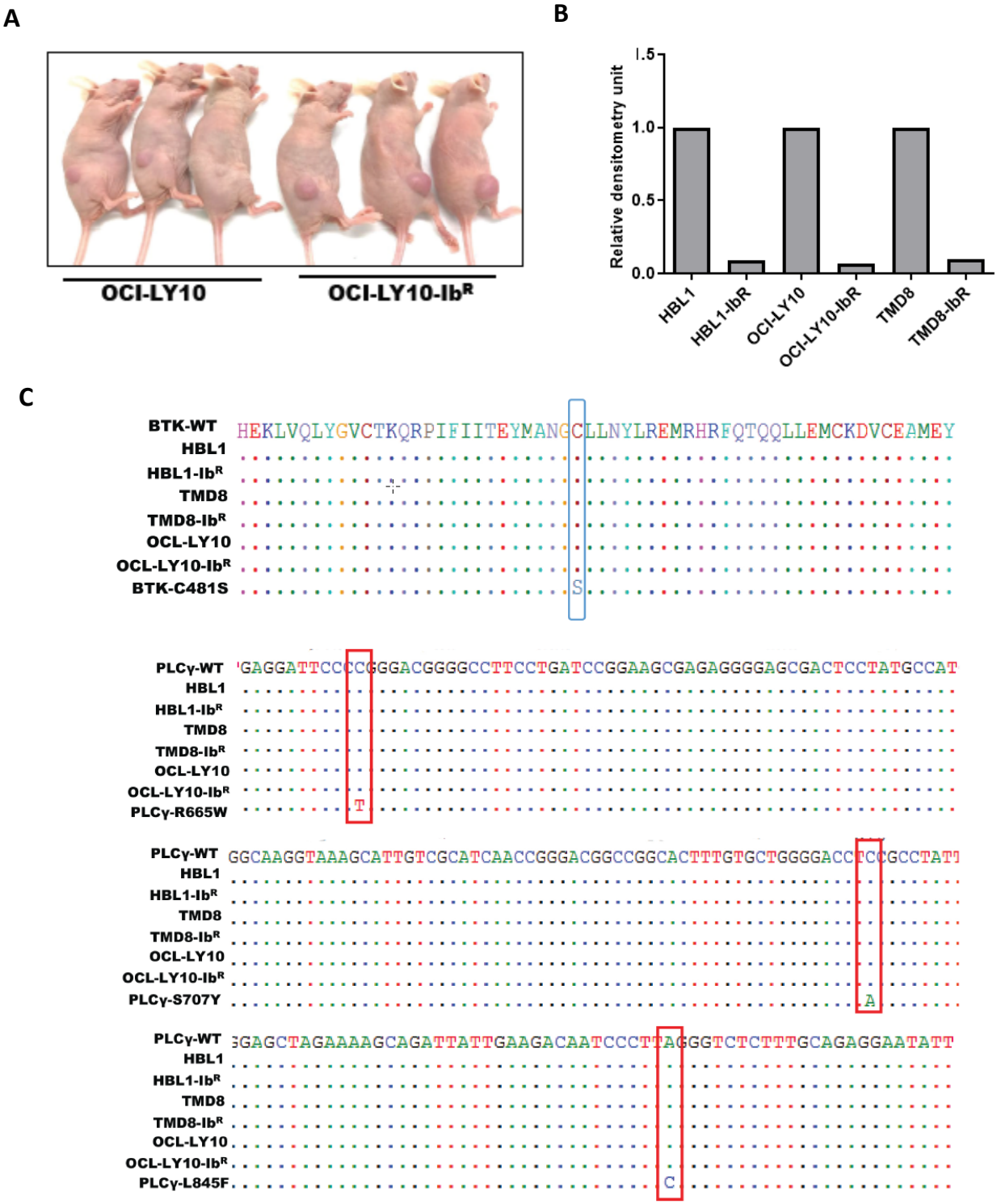

Figure S2.

IR-DLBCL cells and cell proliferation. **A,** OCI-LY10 tumor cells (PT/IR) suspended in a 1:1 Matrigel mixture were implanted subcutaneously into nude mice **B,** Densitometry analyses of BTK expression in IR/parental (PT) DLBCL cells (Fig.2A) **C,** Sequencing of BTK and PLCG2. Targeted sequencing for *BTK* and *PLCG2* mutations was performed in IR- and ibrutinib-sensitive cell lines. No ibrutinib-associated mutations were present in the IR-DLBCL lines examined in this study.

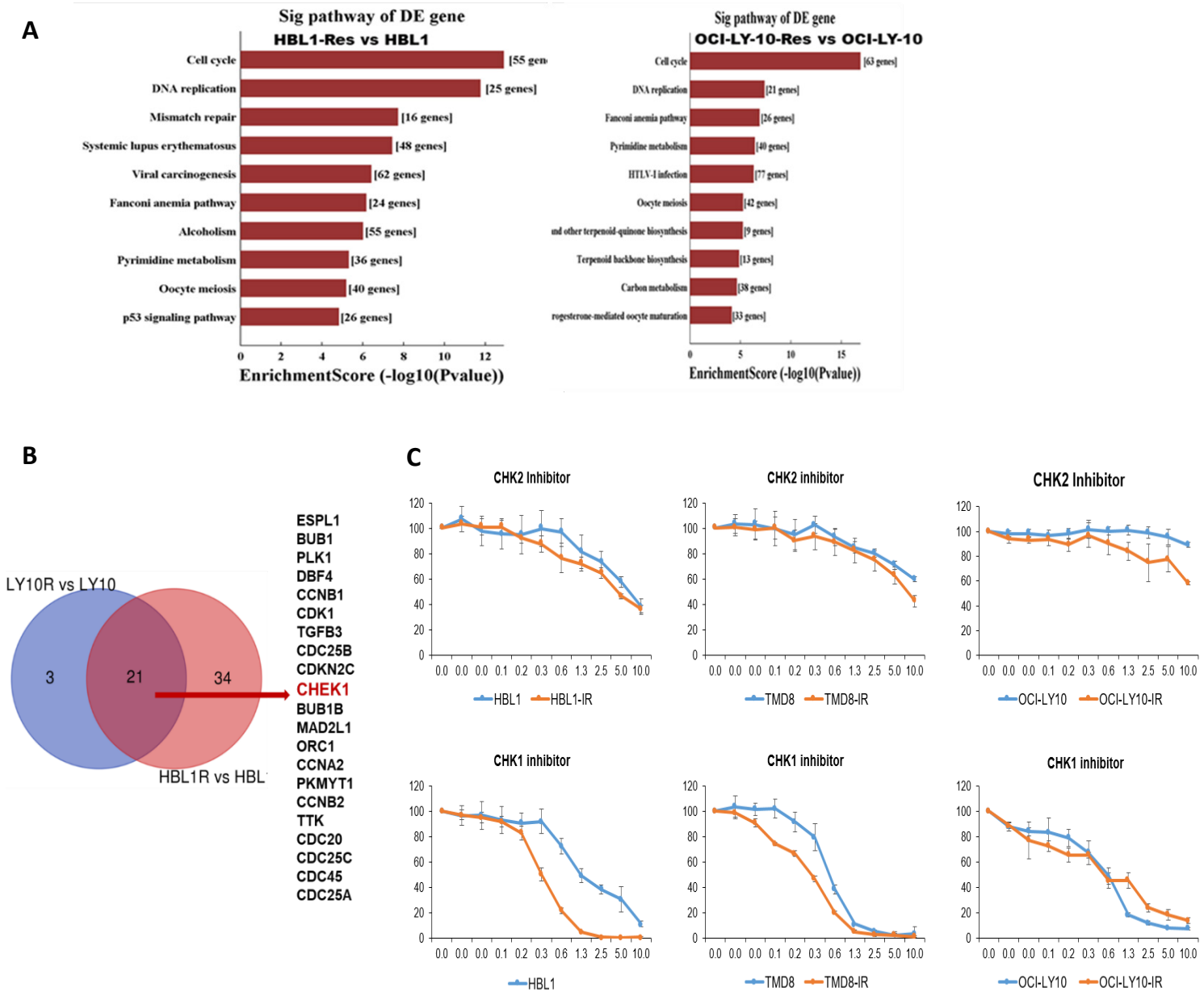

Figure S3.

Differential expression analysis of parental and ibrutinib-resistant DLBCL. **A,** Differential expressed gene (DEG) pathway analysis in all three ibrutinib-resistant (IR) cell lines. **B,** The DEG of cell cycle from each group in (a) were subjected to Venn diagram analyses to identify DEG common to two IR cell lines. CHK1 (in red) is one of the identified DEG. **C,** Treatment with CHK1 or CHK2 inhibitors alone or in combination with ibrutinib did not sensitize IR-DLBCL cells to ibrutinib.

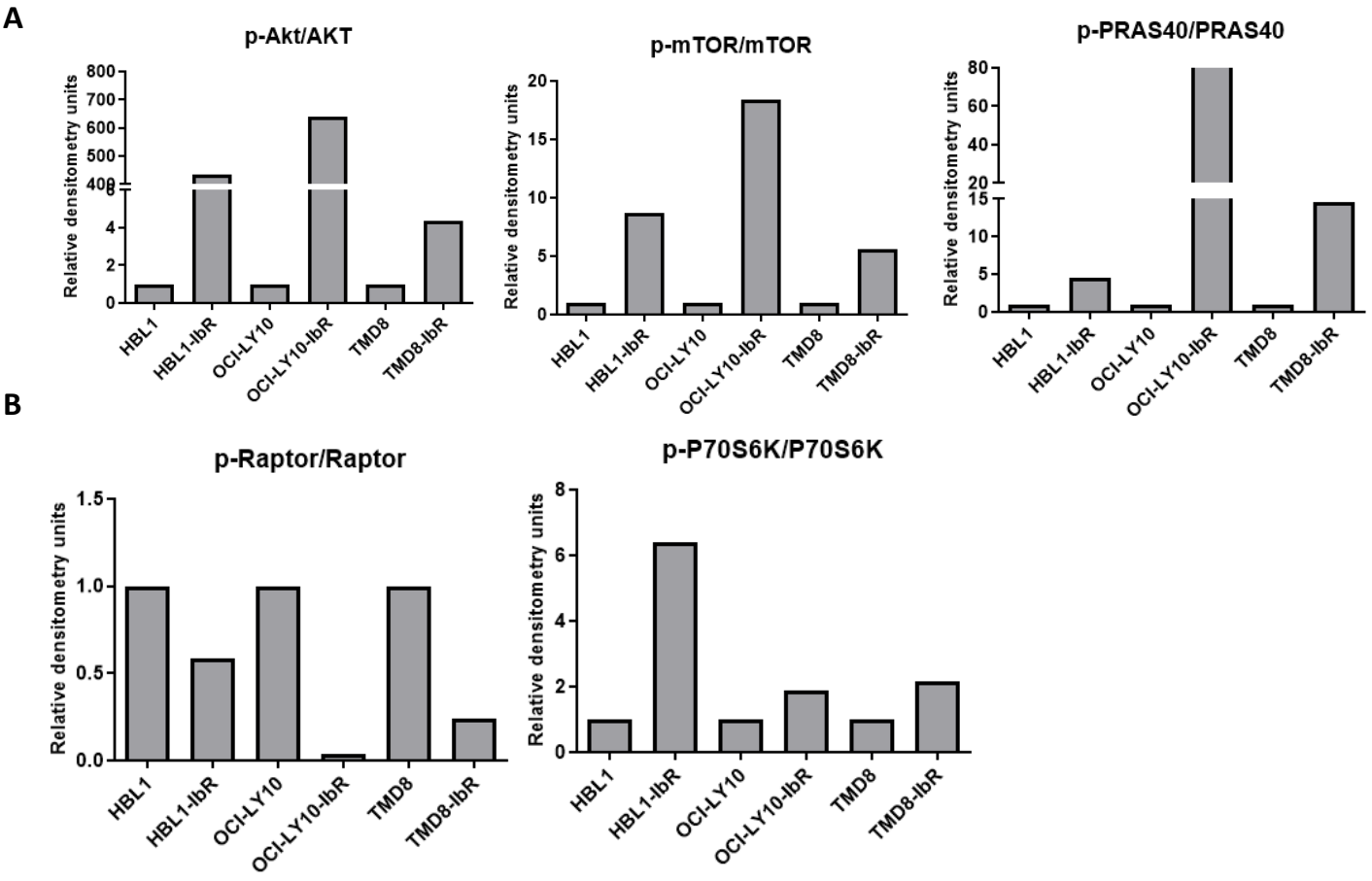

Figure S4.

PI3K pathway is upregulated in ibrutinib-resistant DLBCL. **A-B,** Densitometry analyses for AKT, and mTOR and its substrates (PRAS40, Raptor P70S6K) in ibrutinib-resistant/parental DLBCL cell pairs (shown in Figure 2C).

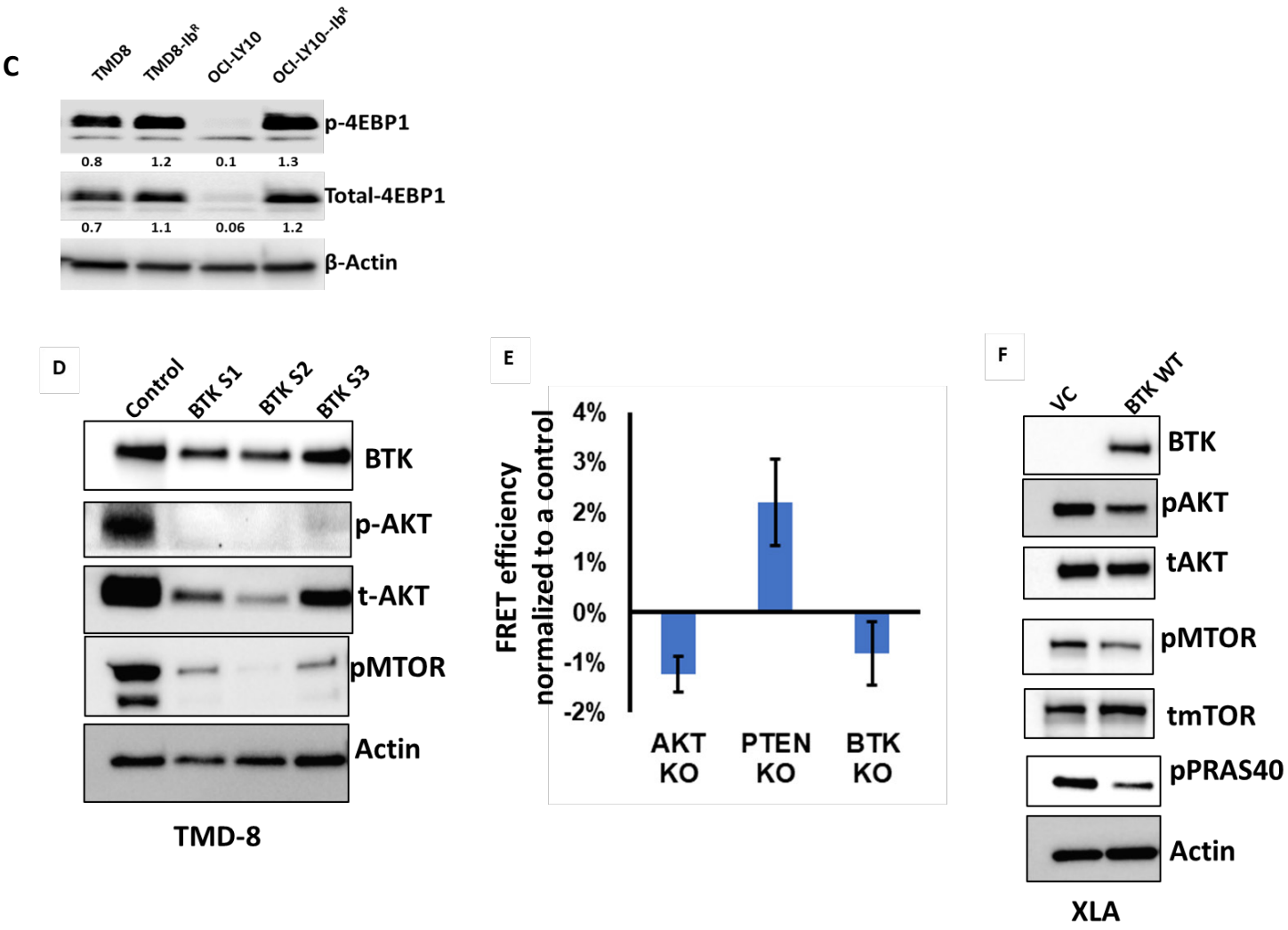

Figure S4.

PI3K pathway is upregulated in ibrutinib-resistant DLBCL. **C,** Western blot analyses demonstrate an increase in total 4EBP1 and p4EBP1 (Thr37/46) levels in ibrutinib-resistant DLBCL along with the densitometry values normalized to actin. **D,** Western blot analyses demonstrate a decrease in total BTK, AKT and pAKT (S473) and pmTOR (S2448) upon transient loss of BTK. **E,** FRET efficiency depicting the active AKT levels in HBL1 cells electroporated with constructs to AKT, PTEN and BTK; note that loss of AKT abrogated AKT activity and loss of PTEN (positive control for AKT activity) increased the levels of AKT phosphorylation. **F,** Western blot analyses demonstrate an increase in total BTK, loss of pAKT and pMTOR upon stable transduction of full length BTK in XLA cells. Note that XLA cells have truncated BTK, that abrogates the expression of BTK.

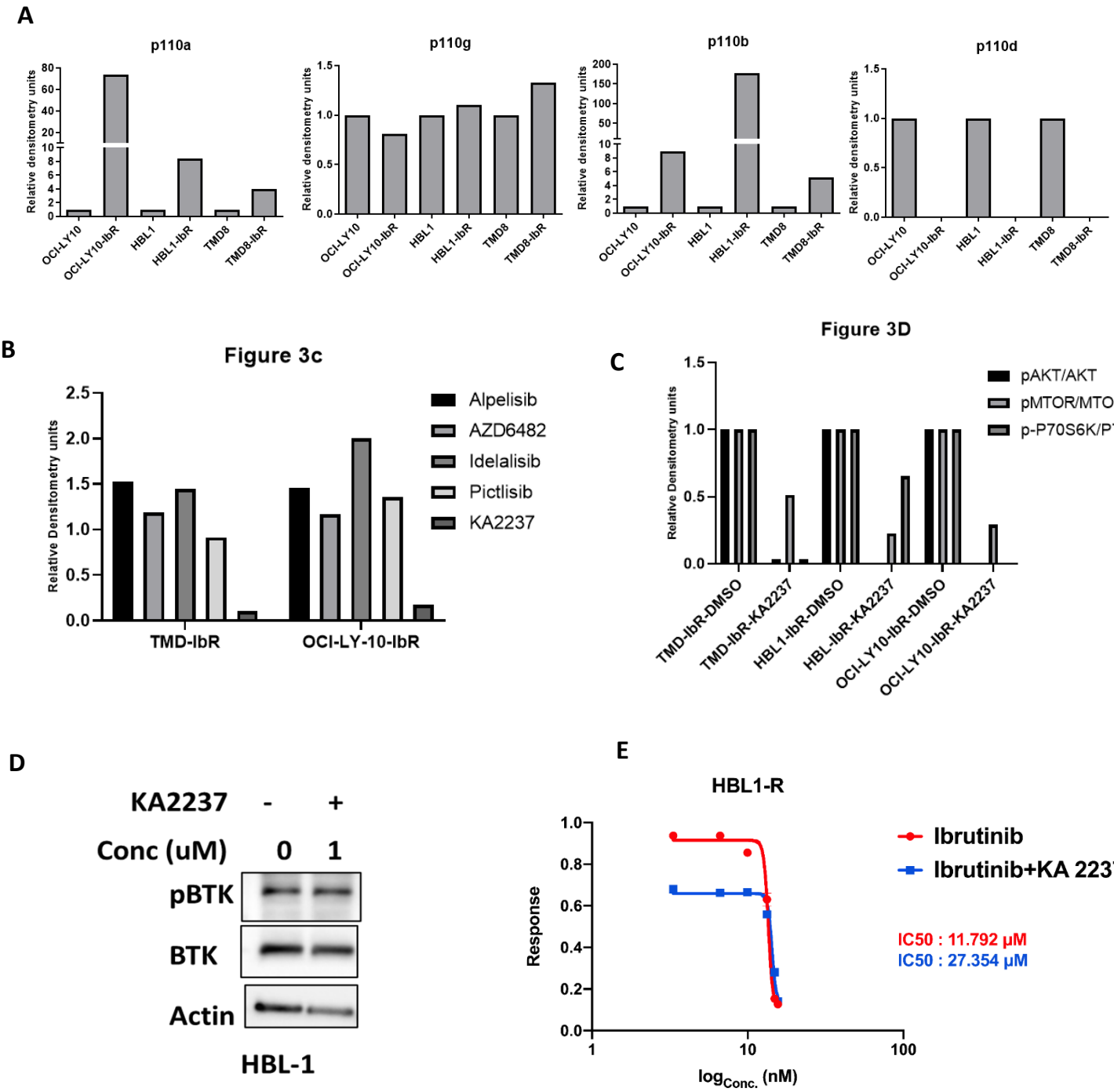

Figure S5.

KA2237 treatment affects expression of PI3K pathway components. **A,** Densitometry analyses of class-I subPI3K isoforms in ibrutinib-resistant (IR) or parental (PT) DLBCL cells. **B,** Quantification of pAKT levels in IR-DLBCL cells after 24 hours of treatment with the indicated inhibitors. **C,** Densitometry analyses for AKT, and mTOR and its substrates (PRAS40, Raptor P70S6K) in IR/PT DLBCL cell pairs after treatment with the PI3K-beta/delta inhibitor. **D,** Western blot analyses demonstrate no change in total BTK and pBTK(Y223) levels upon treatment with 1µM KA2237 for 24hrs. **E,** Dose-response curves and calculated IC50 values for HBL1-Ibrutinib resistant cells upon pre-treatment with KA2237 for 24 hrs prior to exposure to ibrutinib

resistance; IC50 was calculated using MTT. Note that the KA2237 pre-treatment does not sensitize the ibrutinib-resistant cells to ibrutinib.

A

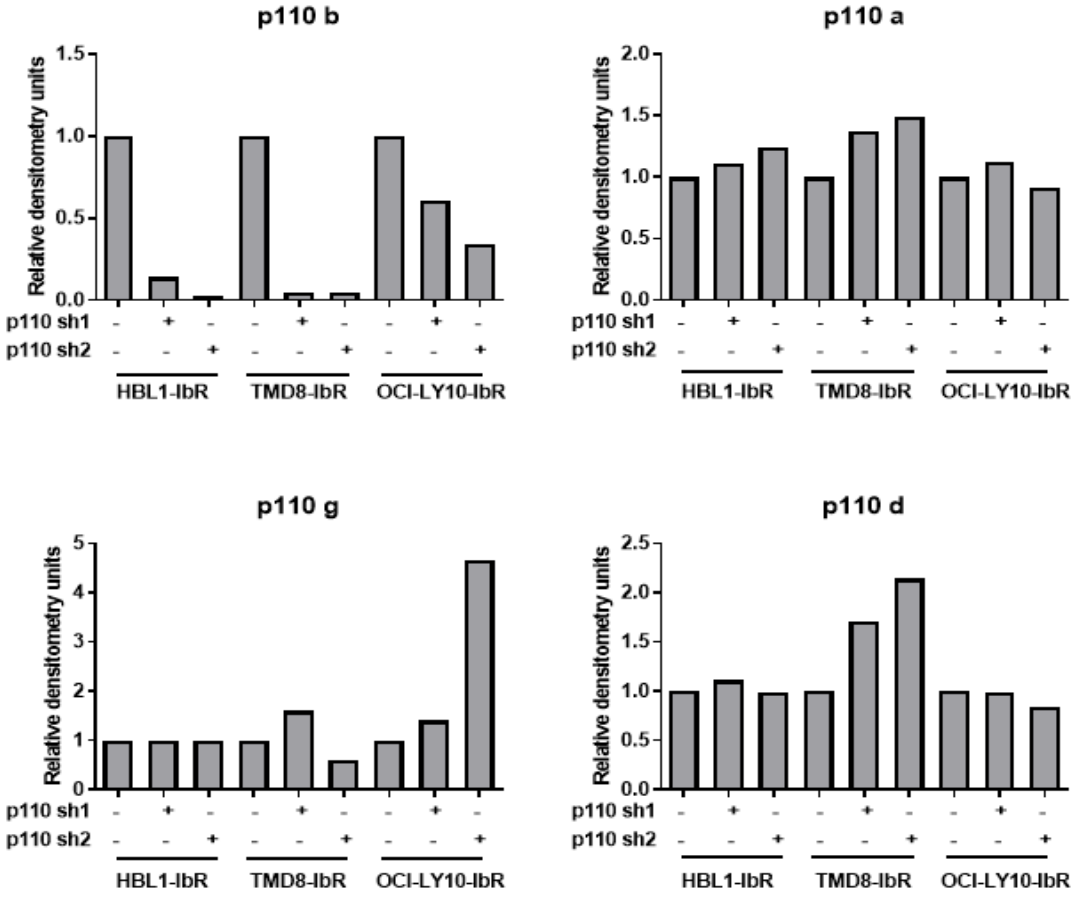

B

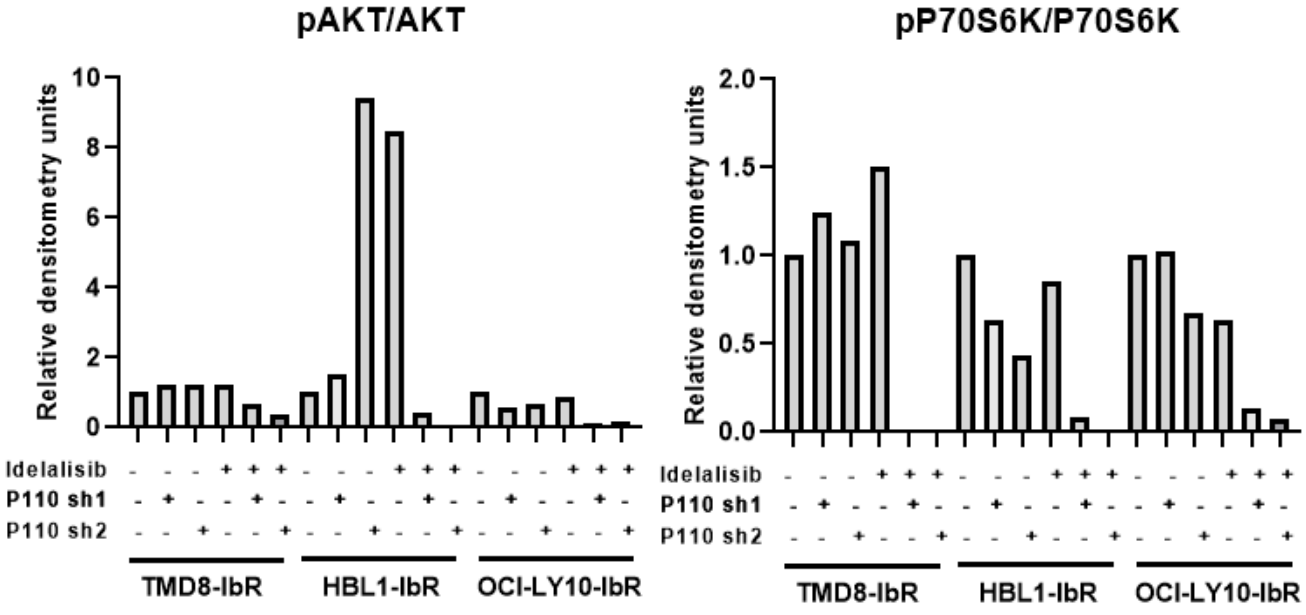

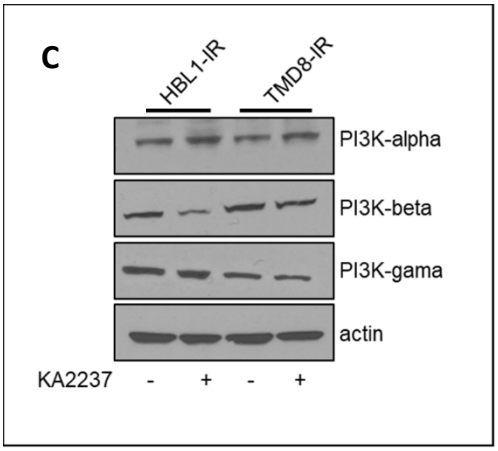

Figure S6. Dual inhibition of p110-beta and -delta in ibrutinib-resistant DLBCL. **A,** Densitometry analyses of PI3K isoforms demonstrate the success of PI3K-beta knockdown in ibrutinib-resistant (IR) DLBCL cell lines. **B,** Quantification of representative pAKT levels and activity of mTOR substrate (P70S6K) in PI3K-beta knockdown IR-DLBCL cells after idelalisib treatment. . **C,** Western blot analyses for PI3K isoform upon treatment with KA2237 at 1μM for 24hrs

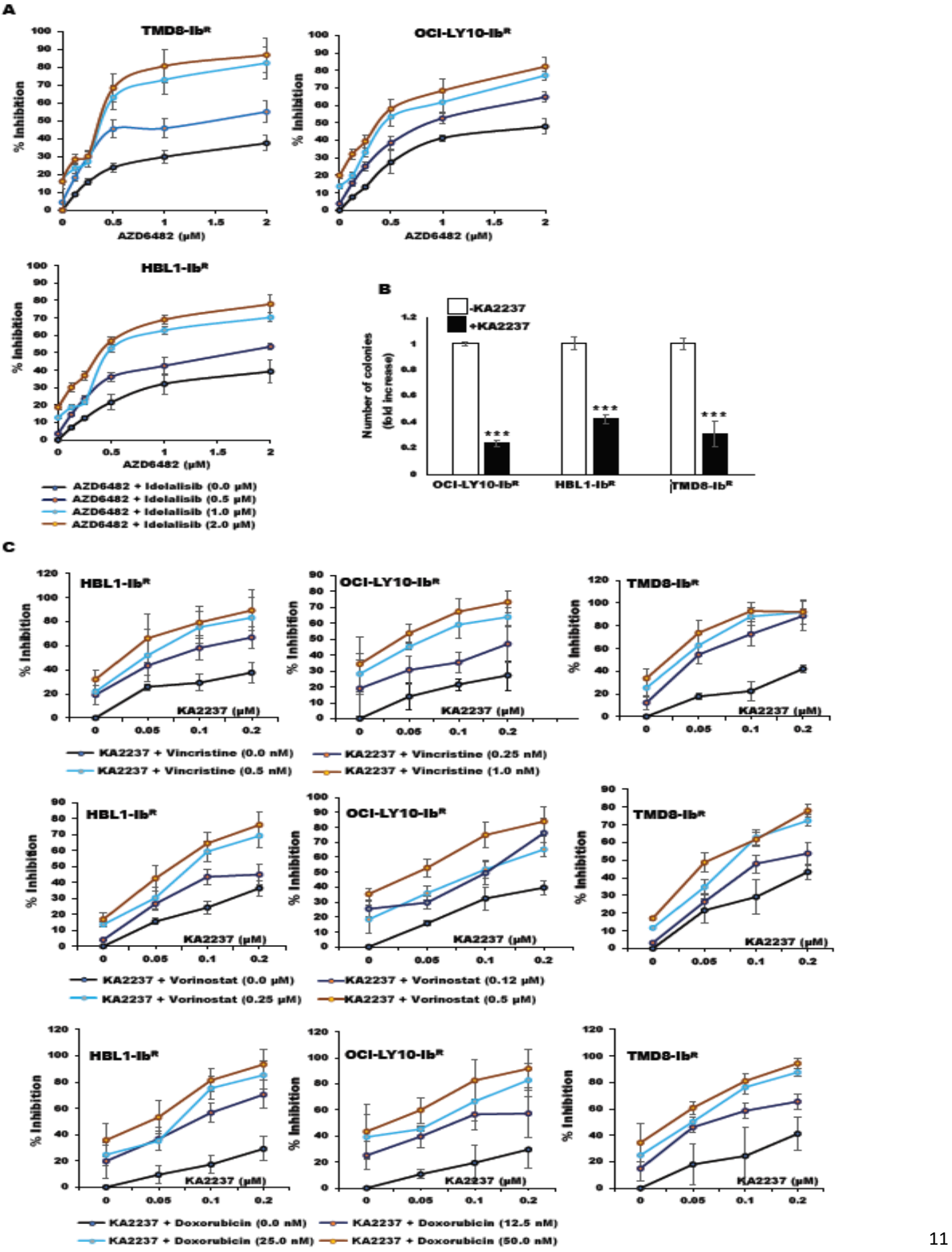
A
TMD8-Ib^R
OCI-LY10-Ib^R
HBL1-Ib^R
% Inhibition
AZD6482 (μM)
AZD6482 + Idelalisib (0.0 μM)
AZD6482 + Idelalisib (0.5 μM)
AZD6482 + Idelalisib (1.0 μM)
AZD6482 + Idelalisib (2.0 μM)
B
-KA2237
+KA2237
Number of colonies (fold increase)
***
OCI-LY10-Ib^R
HBL1-Ib^R
TMD8-Ib^R
C
KA2237 (μM)
KA2237 + Vincristine (0.0 nM)
KA2237 + Vincristine (0.25 nM)
KA2237 + Vincristine (0.5 nM)
KA2237 + Vincristine (1.0 nM)
KA2237 + Vorinostat (0.0 μM)
KA2237 + Vorinostat (0.12 μM)
KA2237 + Vorinostat (0.25 μM)
KA2237 + Vorinostat (0.5 μM)
KA2237 + Doxorubicin (0.0 nM)
KA2237 + Doxorubicin (12.5 nM)
KA2237 + Doxorubicin (25.0 nM)
KA2237 + Doxorubicin (50.0 nM)

D

BEZ	KA2237	Combo	KA2237 (uM)
.00	100.00	100.00	100.00	0.00
.08	38.10	96.70	42.11	0.04
0.16	35.18	87.26	38.70	0.08
0.31	33.26	91.51	35.92	0.16
0.63	31.66	100.21	33.87	0.31
1.25	31.35	85.17	34.54	0.63
2.50	26.36	59.19	29.57	1.25
5.00	28.12	46.67	32.03	2.50
10.00	30.45	45.17	33.90	5.00

TMD8-Ib^R

BEZ (uM)	BEZ	KA2237	Combo	KA2237 (uM)
0.00	100.00	100.00	100.00	0.00
0.08	36.54	92.00	28.80	0.04
0.16	34.69	91.64	32.17	0.08
0.31	30.75	89.11	29.99	0.16
0.63	29.58	84.03	27.75	0.31
1.25	31.62	67.73	28.95	0.63
2.50	26.70	52.73	27.06	1.25
5.00	28.13	43.13	26.76	2.50
10.00	29.92	39.94	28.59	5.00

HBL-Ib^R

Figure S7.

Combining a PI3K-beta/delta dual inhibitor with chemotherapeutic agents. **A,** DLBCL cells exposed to increasing concentrations of PI3K-beta and PI3K-delta inhibitors (AZD6482 and idelalisib). Percent inhibition was calculated, plotted (p<0.05), and compared to untreated cells. **B,** Assay to quantify colony formation in KA2237-treated (+KA2237) and untreated (-KA2237) ibrutinib-resistant (IR) DLBCLs. **C,** IR-DLBCL cells exposed to increasing concentrations of the dual-inhibitor KA2237 plus one of three chemotherapeutic agents; percent inhibition was calculated and plotted, (p<0.05, compared to the only-KA2237 group). **D,** IR-DLBCL cells exposed to increasing concentrations of the dual PI3K/mTOR inhibitor BEZ235 and KA2237, alone or in combination, Drug dose matrix data of IR-DLBCL cells. The numbers in the matrix indicate the percentage of growth inhibition of cells treated with inhibitors (BEZ235 and KA2237) either as single agents or in combination, relative to vehicle-control treated cells. Data were visualized over the matrix using a color scale.

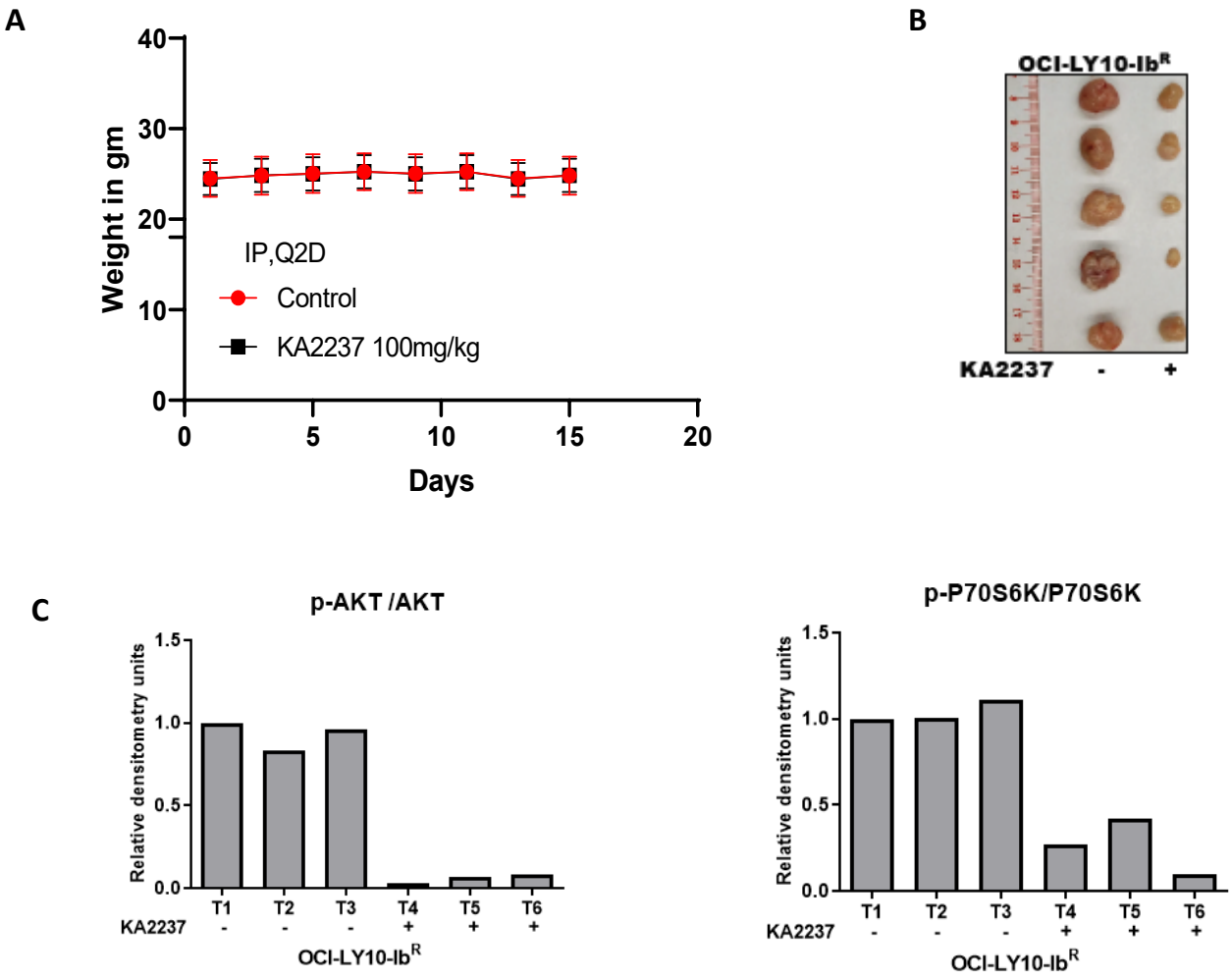

Figure S8.

Dual inhibitor KA2237 exhibits anti-tumor activity in a DLBCL xenograft model. **A,** Mice did not show any toxicity upon KA2237 treatment for 15 days as determined by weight measurements. **B,** Representative images of OCI-LY10-IbR tumor cells treated with KA2237 for 15 days. **C,** Quantification for PI3K/AKT/mTOR signaling pathway from tumor lysates treated with KA2237.

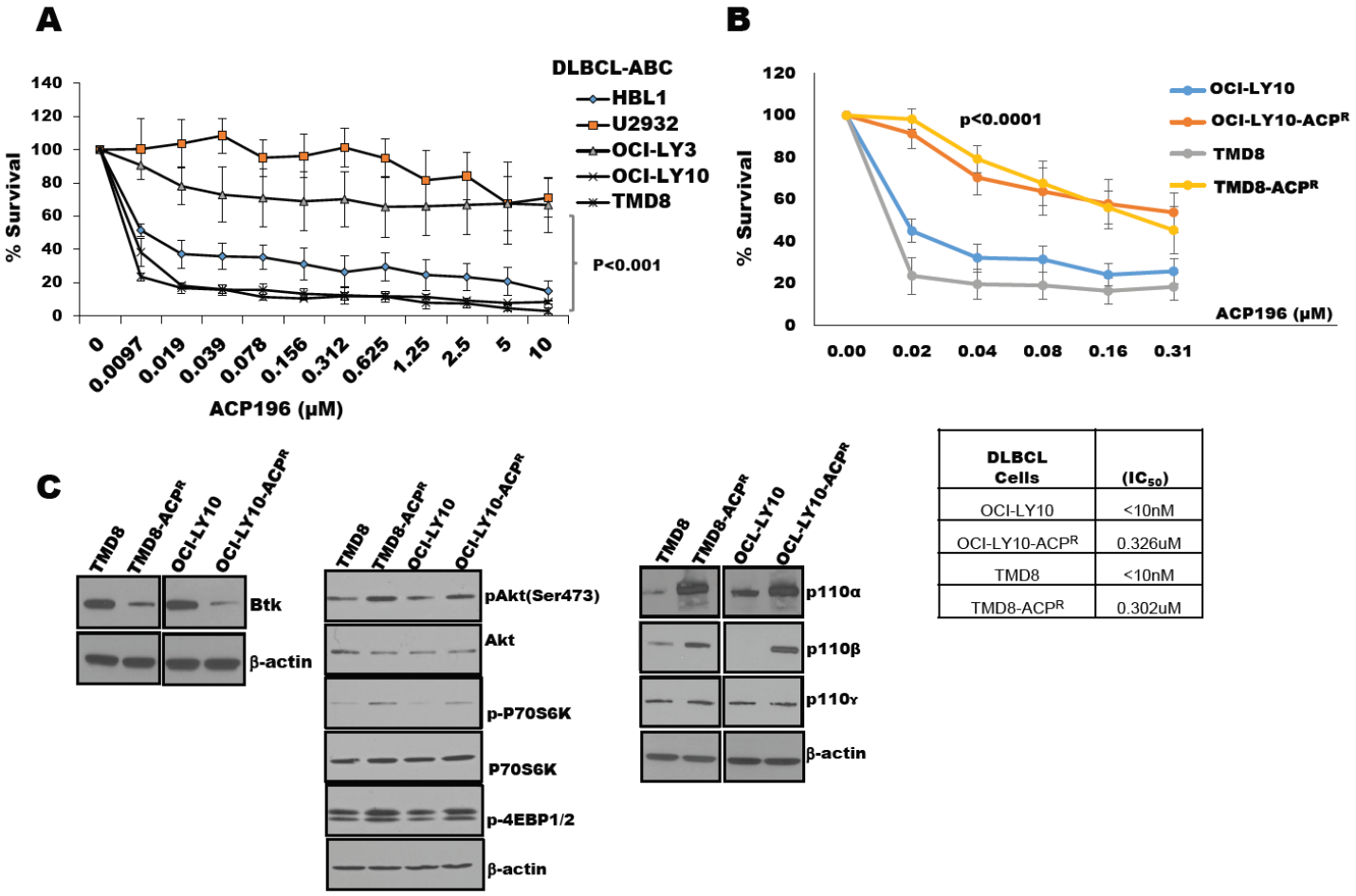

DLBCL Cells	(IC_{50})
OCI-LY10	<10nM
OCI-LY10-ACP^R	0.326uM
TMD8	<10nM
TMD8-ACP^R	0.302uM

Figure S9.

Generation of ACP-196-resistant cell lines. **A,** Three DLBCL cell lines (HBL1, TMD8 and OCI-LY10 were sensitive to ACP196. **B,** ACP-196-resistant cell lines were generated from TMD8 and OCI-LY10 lines using the method previously used to generate ibrutinib-resistant lines. **C,** Western blot analyses showed that ACP-196-resistant cell lines expressed lower levels of BTK, and had enhanced AKT activity, and upregulated expression of PI3K-alpha and -beta isoforms.

Supplementary Tables

Table S1.

Short Tandem Repeat (STR) analysis of ibrutinib and ACP-196-resistant DLBCL cells. **A,** Eight DLBCL cell lines (three IR, their three respective parental-sensitive, and two ACP196-resistant) were analyzed for cell identity by STR. **B,** IC_{50} values of IR-DLBCL cells were determined at different time points after removal of ibrutinib from the culture media. The results indicate stable development of ibrutinib resistance.

A

Source	Sample Name	AMEL	CSF1PO	D13S317	D16S539	D18S51	D21S11	D3S1358	D5S818	D7S820	D8S1179	FGA	TH01	TPOX	vWA	Comments
Lab culture	HBL1	X	10,11	8,9	9,11	14,15,17	30,32	15,16	10,11	11,12	10,13	22,23	6,9	8,9	16,17	
Lab culture	HBL1-Ib^R	X	10,11	8,9	9,11	14,15,17	30,32	15,16	10,11	11,12	10,13	22,23	6,9	8,9	16,17	
CCLC customer database -SET 208	HBL1	X	10,11	8,9	9,11	14,15,17	30,32	15,16	10,11	11,12	10,13	22	6,9	8,9	16,17	MATCH
Lab culture	OCI-LY10	X	11,12	11,12	13	14,18	29	16	10,12	10,11	13,14	20	6,7	8	16,17	
Lab culture	OCI-LY10-Ib^R	X	11,12	11,12	13	14,18	29	16	10,12	10,11	13,14	20	6,7	8	16,17	
Lab culture	OCILY10-ACP^R	X	11,12	11,12	13	14,18	29	16	10,12	10,11	13,14	20	6,7	8	16,17	
CCLC customer database -SET 208	OCI-LY10	X	11,12	11,12	13	14,18	29	16	10,12	10,11	13,14	20	6,7	8	16,17	MATCH
Lab culture	TMD8	X,Y	11,12	9,11	9,11	13,20	30	17,18	12,13	8,10	10,14	17,23	6,7	11	14,18	
Lab culture	TMD8-Ib^R	X,Y	11,12	9,11	9,11	13,20	30	17,18	12,13	8,10	10,14	17,23	6,7	11	14,18	
Lab culture	TMD8-ACP^R	X,Y	11,12	9,11	9,11	13,20	30	17,18	12,13	8,10	10,14	17,23	6,7	11	14,18	
CCLC customer database	TMD8	X,Y	11,12	9,11	9,11	13,20	30	17,18	12,13	8,10	10,14	17,23	6,7	11	14,18	MATCH

B

DLBCL cell lines	IC_{50} µM (0 days)	IC_{50} µM (15 days)	IC_{50} µM (30 days)	IC_{50} µM (45 days)	IC_{50} µM (60 days)
HBL1-Ib^R	1.7	1.8	1.8	1.7	1.2
TMD8-Ib^R	0.51	0.52	0.80	0.53	0.58
OCI-LY10-Ib^R	1.2	1.26	1.58	1.95	1.09

Table S2. Combination index (CI) analysis of PI3K-delta (idelalisib) with PI3K-beta (AZD6482) inhibitor at no-constant ratio in IR-DLBCL cells.

Idelalisib (µM)	AZD6482 (µM)	HBL1-Ib^R		OCI-LY10-Ib^R		TMD8-Ib^R	
		Fa	CI	Fa	CI	Fa	CI
0.50	0.50	0.45	0.19	0.39	0.65	0.36	0.46
0.50	1.00	0.46	0.30	0.53	0.51	0.42	0.54
0.50	2.00	0.55	0.26	0.65	0.44	0.54	0.50
1.00	0.50	0.63	0.09	0.53	0.39	0.52	0.27
1.00	1.00	0.73	0.06	0.62	0.38	0.63	0.23
1.00	2.00	0.82	0.03	0.77	0.24	0.70	0.22
2.00	0.50	0.68	0.11	0.58	0.49	0.57	0.37
2.00	1.00	0.81	0.05	0.68	0.39	0.69	0.26
2.00	2.00	0.87	0.03	0.82	0.23	0.78	0.20

CI values: <0.1, very strong synergism; 0.1-0.3, strong synergism; 0.3-0.7, synergism; 0.7-0.85, moderate synergism; 0.85-0.90, slight synergism; 0.90-1.10, nearly additive. Fa, fraction affected.

Table S3. CI analysis of chemotherapeutic agents with the PI3K-beta/delta inhibitor KA2237 at no-constant ratio in IR-DLBCL cells.

Vorinostat (µM)	**KA2237 (µM)**	**HBL1-Ib^R**		**OCI-LY10-Ib^R**		**TMD8-Ib^R**	
		Fa	**CI**	**Fa**	**CI**	**Fa**	**CI**
0.12	0.05	0.31	0.44	0.31	0.98	0.41	0.50
0.12	0.10	0.47	0.26	0.45	0.58	0.54	0.36
0.12	0.20	0.46	0.45	0.60	0.50	0.57	0.49
0.25	0.05	0.38	0.40	0.29	1.84	0.40	0.69
0.25	0.10	0.66	0.14	0.61	0.29	0.67	0.19
0.25	0.20	0.76	0.10	0.65	0.41	0.75	0.16
0.50	0.05	0.50	0.40	0.46	0.69	0.54	0.45
0.50	0.10	0.71	0.18	0.65	0.25	0.71	0.24
0.50	0.20	0.84	0.10	0.72	0.30	0.81	0.16
Doxorubicin (nM)	**KA2237 (µM)**	**HBL1-Ib^R**		**OCI-LY10-Ib^R**		**TMD8-Ib^R**	
		Fa	**CI**	**Fa**	**CI**	**Fa**	**CI**
12.5	0.05	0.286	0.575	0.347	0.364	0.463	0.309
12.5	0.1	0.532	0.296	0.462	0.408	0.552	0.386
12.5	0.2	0.601	0.36	0.418	0.914	0.591	0.643
25	0.05	0.288	0.79	0.459	0.252	0.548	0.286
25	0.1	0.701	0.195	0.627	0.235	0.768	0.21
25	0.2	0.829	0.132	0.684	0.368	0.847	0.293
50	0.05	0.403	0.783	0.516	0.234	0.598	0.319
50	0.1	0.763	0.232	0.677	0.202	0.811	0.191
50	0.2	0.902	0.109	0.756	0.277	0.909	0.212
Vincristine (nM)	**KA2237 (µM)**	**HBL1-Ib^R**		**OCI-LY10-Ib^R**		**TMD8-Ib^R**	
		Fa	**CI**	**Fa**	**CI**	**Fa**	**CI**
0.25	0.05	0.47	0.22	0.38	0.57	0.47	0.17
0.25	0.10	0.63	0.13	0.52	0.15	0.63	0.11
0.25	0.20	0.76	0.08	0.67	0.05	0.76	0.08
0.50	0.05	0.48	0.24	0.36	1.39	0.54	0.21
0.50	0.10	0.83	0.03	0.68	0.06	0.80	0.06
0.50	0.20	0.92	0.01	0.72	0.04	0.89	0.04
1.00	0.05	0.64	0.11	0.53	0.46	0.64	0.24
1.00	0.10	0.85	0.02	0.72	0.06	0.85	0.06
1.00	0.20	0.97	0.00	0.79	0.03	0.97	0.01

CI values: <0.1, very strong synergism; 0.1-0.3, strong synergism; 0.3-0.7, synergism; 0.7-0.85, moderate synergism; 0.85-0.90, slight synergism; 0.90-1.10, nearly additive. Fa, fraction affected.

1. Havranek O, Xu J, Kohrer S, et al. Tonic B-cell receptor signaling in diffuse large B-cell lymphoma. *Blood*. 2017;130(8):995-1006.
2. Kowarz E, Loscher D, Marschalek R. Optimized Sleeping Beauty transposons rapidly generate stable transgenic cell lines. *Biotechnol J*. 2015;10(4):647-653.
3. Cong L, Ran FA, Cox D, et al. Multiplex genome engineering using CRISPR/Cas systems. *Science*. 2013;339(6121):819-823.
4. Ran FA, Hsu PD, Wright J, Agarwala V, Scott DA, Zhang F. Genome engineering using the CRISPR-Cas9 system. *Nat Protoc*. 2013;8(11):2281-2308.